Supplementary Material
A handful of co-active synapses is sufficient to drive principal neurons along the hippocampal trisynaptic circuit.

Alessandro Fiasconaro[1,2,3], Pierpaolo Arenare[1], Michele Migliore[1,4], and Rosanna Migliore[1,*]

[1]Institute of Biophysics, National Research Council, Palermo, Italy
[2]Department of Condensed Matter Physics, University of Zaragoza, Zaragoza, Spain
[3]Institute for Biocomputation and Physics of complex Systems, University of Zaragoza, Zaragoza, Spain
[4]European Brain Research Institute-Fondazione Rita Levi-Montalcini, Rome, Italy
[*]Corresponding author: Rosanna Migliore. e-mail: rosanna.migliore@cnr.it

1 Short-term plasticity in the three neurons

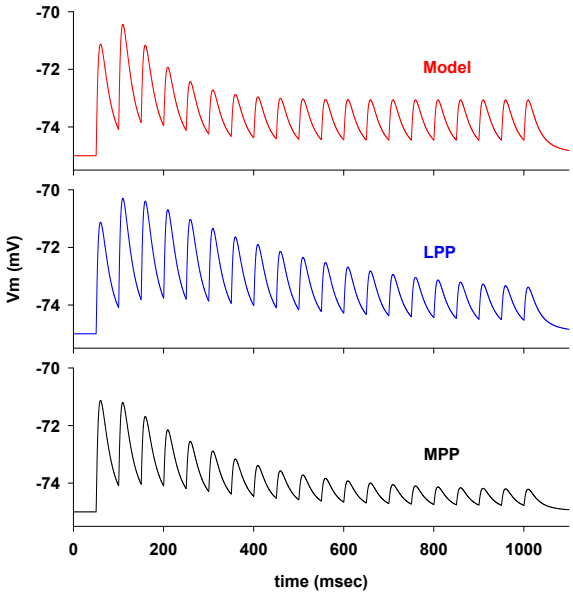

Supplementary figure 1. Short-term plasticity at the EC-DG perforant path synapse. Membrane potential responses recorded in current clamp from a passive single-compartment cell ($R_{in} \approx 255\,M\Omega, \tau_m = 20\,ms, V_{rest} = -75\,mV$) in response to a train of 20 stimuli delivered at 20 Hz. Synaptic dynamics were modeled using the Tsodyks–Markram framework[1,2], in which short-term plasticity is described by three parameters: U, the synaptic utilization; τ_f, the facilitation time constant; and τ_d, the recovery time constant from depression. Responses are shown for the parameter set used in this study (Model, red; $U = 0.30, \tau_f = 80\,ms$, and $\tau_d = 350\,ms$) and for parameter sets derived from the experimental findings for lateral (LPP, blue; $U = 0.093, \tau_f = 29\,ms, \tau_d = 1624\,ms$) and medial perforant path data (MPP, black; $U = 0.191, \tau_f = 7\,ms, \tau_d = 1539\,ms$) reported by Petersen et al.[3] in Fig. 6B. Synaptic weights were scaled such that the first response had the same amplitude across conditions. The model produced a slight increase in synaptic efficacy at the second stimulus (paired-pulse ratio, PPR = 1.02), followed by depression from the third stimulus onward. This response profile lies between those obtained with the LPP- and MPP-derived parameter sets and is consistent with the range of short-term plasticity reported experimentally by Petersen et al., who measured PPRs of 1.28 (LPP) and 0.81 (MPP) for EPSCs, and 1.24 (LPP) and 1.07 (MPP) for fEPSPs. Together, these results support the use of the model as a reasonable representation of EC–DG synaptic dynamics.

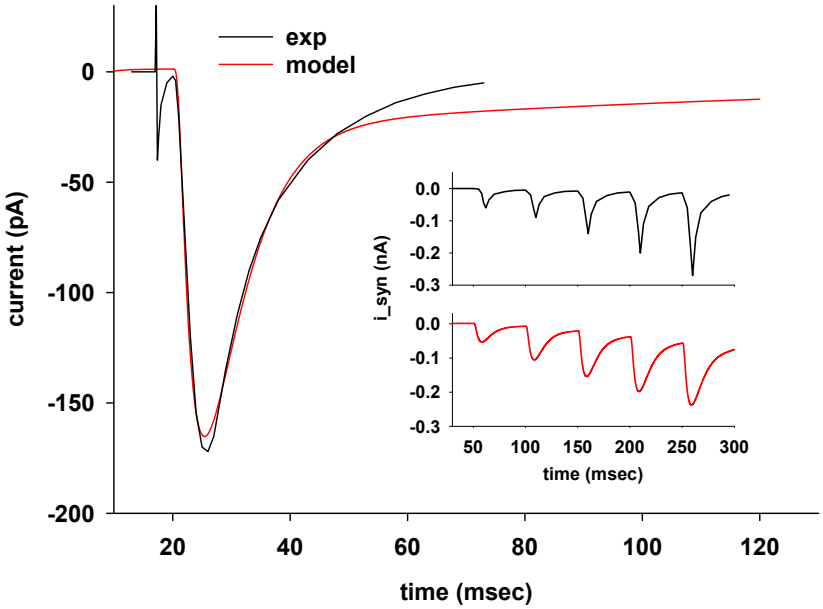

Supplementary figure 2. Short-term plasticity at the DG-CA3 mossy fiber synapse. EPSCs recorded in voltage clamp ($V_h = -60 mV$) from a simplified model cell following mossy fiber stimulation. Main panel: EPSC evoked by a single stimulus. Black: experimental trace digitized from Henze et al.[4], Fig. 4A. Red: model. The fast transient at ~ 17 ms in the experimental trace is a stimulus artifact and was ignored by the fitting procedure. Inset: EPSCs evoked by a train of five stimuli delivered at 20 Hz; experimental data (black) were digitized from Fig. 3A of Toth et al.[5] and model responses are shown in red. Simulations were performed in NEURON at 24 °C using a model cell consisting of a somatic compartment (L = diam = 20 μm) connected to a passive dendrite. The synapse was placed at the distal dendritic end, and synaptic currents were recorded at the soma using a single-electrode voltage clamp. Short-term dynamics were described by the Tsodyks–Markram model[1,2], with utilization of synaptic efficacy $U = 0.0236$, facilitation time constant $\tau_f = 544$ ms, and time constant of recovery from depression $\tau_d = 300$ ms. The NMDA/AMPA ratio was 1.23, with $E_{syn} = 0$ mV; NMDA conductances included voltage-dependent Mg^{2+} block with $[Mg^{2+}]_o = 1$ mM[8]. The same synaptic parameters were used for both experimental protocols, whereas dendritic passive properties and synaptic weight were fitted independently for each dataset, reflecting the different experimental preparations, using Nelder–Mead minimization of the root-mean-square (RMS) error. For the single-EPSC dataset, the fitted dendrite had $L = 922\,\mu$m and diameter $= 4.76\,\mu$m, yielding an RMS error of 6.3 pA after exclusion of the stimulation artifact and a model peak amplitude of -165 pA compared with -172 pA experimentally. For the stimulus train, the fitted dendrite had $L = 499\,\mu$m and diameter $= 5.0\,\mu$m; peak samples were weighted six-fold during fitting, and the model peak amplitudes ranged from 88% to 117% of the corresponding experimental values. The ability of the same Tsodyks–Markram synaptic parameters to reproduce both the single-EPSC waveform and the short-term dynamics evoked by repetitive stimulation provides support for the model as a reasonable representation of mossy fiber synaptic transmission in the DG–CA3 circuit.

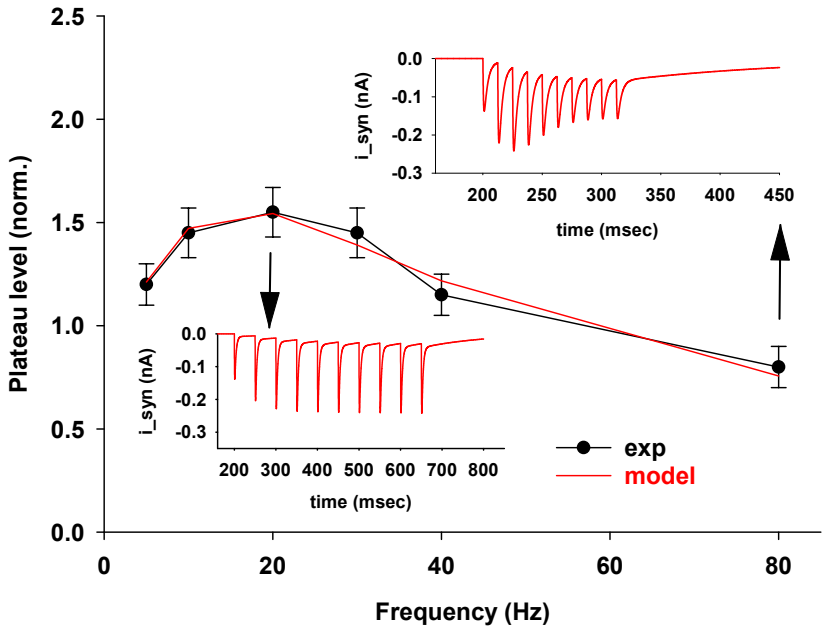

Supplementary figure 3. Short-term plasticity at the CA3-CA1 Schaffer collateral synapse. Plateau levels of excitatory postsynaptic currents (EPSCs) evoked by trains of 10 stimuli delivered at frequencies ranging from 5 to 80 Hz, recorded under voltage clamp ($V_h = -70$ mV). Experimental data (black filled circles) from Schaffer collateral–CA1 pyramidal cell synapses were obtained from Wierenga and Wadman[6] (n=10); error bars indicate the SEM. Model simulations using the Tsodyks–Markram (TM) framework[1,2] are shown in red. Insets show simulated EPSC trains at 20 Hz (lower left) and 80 Hz (upper right). The plateau level was calculated as the mean normalized amplitude of the eighth to tenth EPSCs in each train. Individual EPSC amplitudes were measured as the difference between the peak current and the local baseline, defined as the current measured 0.2 ms before stimulus onset, and normalized to the amplitude of the first EPSC in the train, following Wierenga and Wadman[6]. The synaptic model, implemented in NEURON, included AMPA and NMDA conductances[7], with voltage-dependent Mg^{2+} block[8] ($[Mg^{2+}]_o = 1.0$ mM) and an NMDA/AMPA conductance ratio of 1.23[9]. TM short-term plasticity parameters were optimized by differential evolution against the experimental plateau levels from Wierenga and Wadman (Fig. 4A) and paired-pulse ratios (Fig. 4B)[6], using a weighted χ^2 cost function. Optimization yielded U=0.1528, $\tau_f = 138.4$ ms, and $\tau_d = 101.0$ ms. The close agreement between simulated and experimental plateau levels across stimulation frequencies supports the ability of the TM model to reproduce the frequency-dependent short-term plasticity of the CA3–CA1 Schaffer collateral synapse, including the non-monotonic response characterized by facilitation up to 20 Hz followed by depression at higher frequencies.

2 CA3 non adaptive/bursting configurations

As indicated in Fig. 1 of the MD, the cell is optimized with three different channel configurations in such a way to reproduce three distinct traces in output, with the following features: *Adapting* spike output, *non-adapting*, and *bursting*. The main document only reports the outcomes of the CA3 in the *adapting* configuration, which we consider the most important and mainly representative of the cell. Here we report, for completeness, the results concerning both the *non-adapting* and the *bursting* configurations of the same morphology.

The figures here reproduced concern the two latter cell-types, with the same types of plot inserted in the main manuscript. We can observe how a small increase of depolarization in the case of potential lock can give rise a high frequency signaling, as demonstrated by the traces on the right hand side, of the plots, where an almost constant value of the membrane potential, still registers a spiking behavior which increases the frequency records.

The results of the *bursting* configuration are very similar, almost superimposable, to those of the *adapting* configuration reported in the main manuscript.

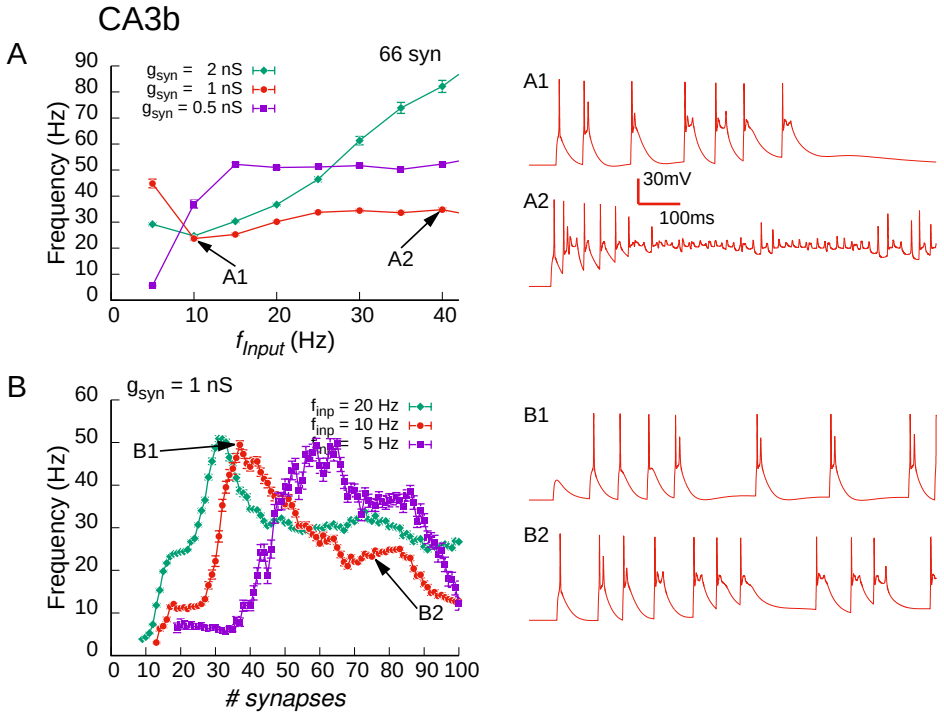

Supplementary figure 4. Results of the CA3 cell in the *bursting* configuration. Panel A: output frequency of the cell as a function of the input frequency f_{inp} for the maximum synapses' conductivities $g_{\mathrm{syn}} = 0.5, 1$, and 2 nS in the case of 66 excitatory synapses arriving on the cell. The panels A1 and A2 on the right hand side report an example of the traces indicated in the corresponding plot. Panel B: Frequency output as a function of the number of arriving synapses for different input frequencies ($F_{inp} = 5, 10, 20$Hz) at the experimental value of synapse conductance $g_{\mathrm{syn}} = 1$ nS. The cell presents a strong nonmonotonic behavior with a reduction of output frequency by increasing the number of synapses. This implies a clear maximum possible spiking rate with the loss of transfer information for increasing number of synapses on the CA3 bursting neuron.

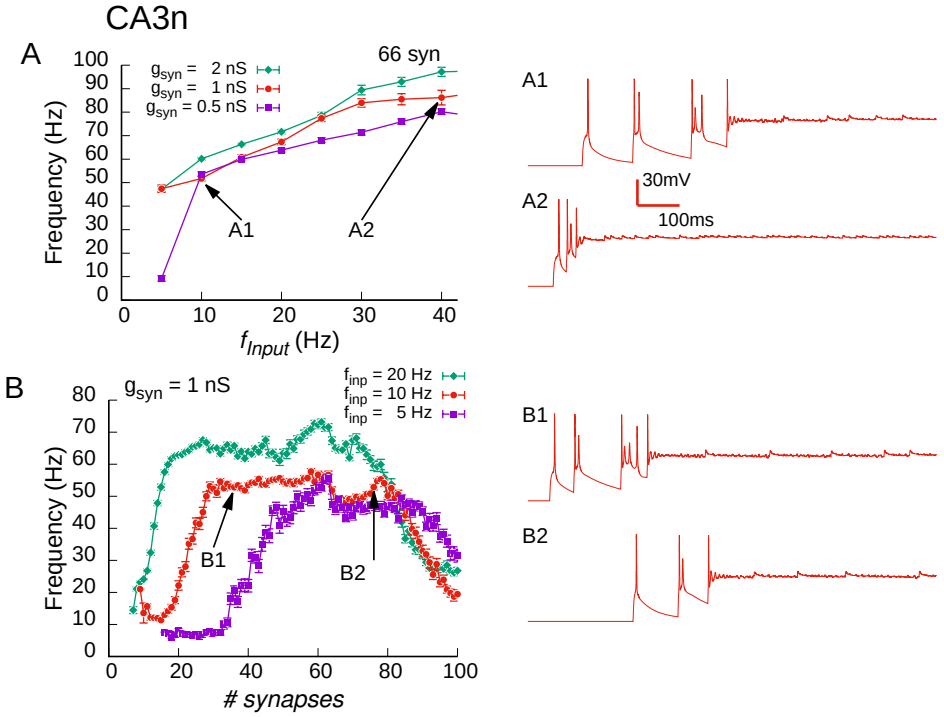

Supplementary figure 5. Results of the CA3 cell in the *non adapting* configuration. The same type of plot of Fig. 4. In panel A we observe a very high increase of spiking rate for all the synaptic weights considered, while again a strong nonmonotonic behavior in the frequency output as a function of the number of synapses is visible in panel B, with the presence of a large plateau region.

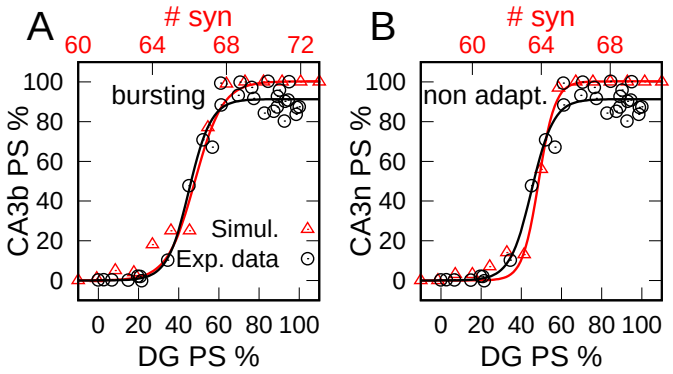

Supplementary figure 6. Postsynaptic activation probability for the *bursting* (panel A) and *non adapting* (panel B) configurations of the CA3 cell. Each panel reports the probability of generating a spike as a function of the presynaptic population spike percentage measured experimentally by Bartesaghi et al.[10] (lower x-axis, black circles) and the number of synaptic contacts used in the simulations (upper x-axis, red triangles). Simulations were computed from 100 trials with random synaptic placement for each condition. Sigmoidal fits were applied to both experimental and simulation data and aligned at the midpoint of the transition between no activation and full activation, allowing a direct comparison between the experimental presynaptic activation percentage and the number of synaptic contacts in the simulations. The *bursting* case appears very similar to the *adapting* configuration reported in the main manuscript, while the *non-adapting* presents a slightly lower activation threshold –around 2 synapses less– than the two other cases.

3 Activation probability.

This paragraph reports in Table 1 the complete set of parameters values obtained by fitting the activation probability according to both the experiments and the simulation (in terms of presynaptic activation percentage and of the number of arriving synapses, respectively) presented in Fig. 9 of the main manuscript. The fitted function is the sigmoid

$$f(x) = \frac{a}{1 + e^{b(c^* - x)}}. \tag{1}$$

Supplementary table 1. Fit parameters related to Fig. 9 of the main manuscript.

Stage	Saturation a_{EXP}	Slope b_{EXP}	Midpoint c^*_{EXP}	Saturation a_{Model}	Slope b_{Model}	Midpoint c^*_{Model}
EC→DG	92.8	0.29	37.4	99.7	0.52	9.15
DG→CA3a	91.3	0.18	45.2	100.2	1.61	66.2
DG→CA3b	91.3	0.18	45.2	100.3	1.33	66.3
DG→CA3n	91.3	0.18	45.2	100.3	2.11	63.9
CA3→CA1	92.0	0.16	52.5	100.0	0.67	5.30

References

1. Tsodyks MV, Markram H. The neural code between neocortical pyramidal neurons depends on neurotransmitter release probability. *Proc Natl Acad Sci* USA. 1997; 94(2):719-23. doi: 10.1073/pnas.94.2.719. Erratum in: Proc Natl Acad Sci U S A 1997;94(10):5495. PMID: 9012851; PMCID: PMC19580.
2. Tsodyks M, Pawelzik K, Markram H. Neural networks with dynamic synapses. *Neural Comput.* 1998; 10(4):821-35. doi: 10.1162/089976698300017502. PMID: 9573407.
3. Petersen RP, Moradpour F, Eadie BD, Shin JD, Kannangara TS, Delaney KR, Christie BR. Electrophysiological identification of medial and lateral perforant path inputs to the dentate gyrus. *Neuroscience.* 2013; 252:154-68. doi: 10.1016/j.neuroscience.2013.07.063. Epub 2013 Aug 7. PMID: 23933307.
4. Henze DA, Urban NN, Barrionuevo G. The multifarious hippocampal mossy fiber pathway: a review. *Neuroscience.* 2000;98(3):407-27. doi: 10.1016/s0306-4522(00)00146-9.
5. Toth K, Suares G, Lawrence JJ, Philips-Tansey E, McBain CJ. Differential mechanisms of transmission at three types of mossy fiber synapse. *J Neurosci.* 2000;20(22):8279-89. doi: 10.1523/JNEUROSCI.20-22-08279.2000. PMID: 11069934; PMCID: PMC6773175.
6. Wierenga CJ, Wadman WJ. Excitatory inputs to CA1 interneurons show selective synaptic dynamics. *J Neurophysiol.* 2003;90(2):811-21. doi: 10.1152/jn.00865.2002. PMID: 12904494.
7. Andrasfalvy BK, Magee JC. Distance-dependent increase in AMPA receptor number in the dendrites of adult hippocampal CA1 pyramidal neurons. *J Neurosci.* 2001;21(23):9151-9. doi: 10.1523/JNEUROSCI.21-23-09151.2001. PMID: 11717348; PMCID: PMC6763889
8. Jahr CE, Stevens CF. Voltage dependence of NMDA-activated macroscopic conductances predicted by single-channel kinetics. *J Neurosci.* 1990;10(9):3178-82. doi: 10.1523/JNEUROSCI.10-09-03178.1990. PMID: 1697902; PMCID: PMC6570236.
9. Le Roux N, Cabezas C, Böhm UL, Poncer JC. Input-specific learning rules at excitatory synapses onto hippocampal parvalbumin-expressing interneurons. *J Physiol.* 2013;591(7):1809-22. doi: 10.1113/jphysiol.2012.245852. PMID: 23339172; PMCID: PMC3624852.
10. Bartesaghi R, Migliore M, & Gessi T. Input-output relations in the entorhinal cortex-dentate-hippocampal system: evidence for a non-linear transfer of signals. *Neuroscience* 2006;142(1):247–265. doi: 10.1016/j.neuroscience.2006.06.001.